

Use of Atmospheric Infrared Sounder high-spectral resolution spectra to assess the calibration of Moderate resolution Imaging Spectroradiometer on EOS Aqua

David C. Tobin,¹ Henry E. Revercomb,¹ Christopher C. Moeller,¹ and Thomas S. Pagano²

Received 19 April 2005; revised 19 August 2005; accepted 20 October 2005; published 31 March 2006.

[1] AIRS and MODIS on the EOS Aqua spacecraft collect global observations of the Earth's upwelling infrared radiance for numerous remote sensing and climate related applications. This paper presents comparisons of the AIRS and MODIS radiance observations and illustrates the utility of using high-spectral resolution observations to create a highly accurate assessment of broadband sensor calibration. In the analysis, the high-spectral resolution AIRS spectra are reduced to MODIS spectral resolution, and the high-spatial resolution MODIS data are reduced to AIRS spatial resolution for global data collected on 6 September 2002 and 18 February 2004. Spatially uniform scenes are selected, and the observed differences are characterized as a function of several parameters including scene temperature, sensor scan (view) angle, and solar zenith angle. The comparisons are in general very good with respect to the expected radiometric accuracies of the sensors, with mean brightness temperature differences of 0.1 K or less for many of the MODIS bands. Uncertainties of these determinations range from near 0 K for window region bands to as large as 0.2 K for other bands. For MODIS water vapor bands 27 (6.8 μm) and 28 (7.3 μm) and temperature sounding bands 34 (13.7 μm), 35 (13.9 μm), and 36 (14.2 μm), the differences exhibit a dependence on scene temperature, with peak differences exceeding 1 K for bands 27 and 36. Differences as a function of scan angle are 0.4 K or less for all bands, and scan angles but clear trends are defined. Results for the 2 days demonstrate good reproducibility with changes in mean differences of 0.1 K or less for most bands.

Citation: Tobin, D. C., H. E. Revercomb, C. C. Moeller, and T. S. Pagano (2006), Use of Atmospheric Infrared Sounder high-spectral resolution spectra to assess the calibration of Moderate resolution Imaging Spectroradiometer on EOS Aqua, *J. Geophys. Res.*, *111*, D09S05, doi:10.1029/2005JD006095.

1. Introduction

[2] The Atmospheric Infrared Sounder (AIRS) and the Moderate resolution Imaging Spectroradiometer (MODIS) on the sun synchronous polar orbiting NASA's Earth Observing System (EOS) Aqua platform measure the upwelling infrared radiance of the earth and its atmosphere for numerous remote sensing and climate related applications [Parkinson, 2003]. AIRS [Aumann *et al.*, 2003] is a hyperspectral grating spectrometer which measures the thermal infrared spectrum with 2378 spectral channels covering the 3.75–4.59 μm (2181–2665 cm^{-1}), 6.20–8.22 μm (1217–1614 cm^{-1}), and 8.8–15.4 μm (650–1136 cm^{-1}) spectral regions with resolving power ($\lambda/\Delta\lambda$) ranging from 1080 to 1590. It has infrared footprints approximately 13.5 km in diameter at nadir and utilizes cross track scanning to collect

90 cross track footprints every 2.667 s with a swath width of ~ 1650 km. MODIS [Barnes *et al.*, 1998] is a high-spatial resolution, multispectral cross track scanning radiometer with 16 infrared spectral bands with spectral centroids ranging from 3.78 to 14.22 μm (703 to 2649 cm^{-1}) and resolving power ranging from 20 to 50. The infrared footprints are 1 km in diameter at nadir and cross track scanning of 10 along-track detectors per spectral band is used to collect 1354 cross track samples yielding a ~ 2320 km swath. Figure 1 displays a sample AIRS brightness temperature spectrum measured on 18 February 2004 at 1629 UTC overlaid with the Aqua MODIS detector averaged Spectral Response Functions (SRFs). Central wavelengths and bandwidths of the MODIS spectral bands are also listed in Table 1.

[3] Both AIRS and MODIS have high radiometric accuracy requirements for achieving their climate and remote sensing goals. In addition to extensive prelaunch characterization of the sensors, there have been several postlaunch validation studies focused on characterization of AIRS [e.g., Aumann *et al.*, 2003; Pagano *et al.*, 2003; Revercomb *et al.*, 2003; Tobin *et al.*, 2003, 2006; Larar *et al.*, 2005; H. H. Aumann *et al.*, unpublished manuscript, 2006] and

¹Cooperative Institute for Meteorological Satellite Studies, Space Science and Engineering Center, University of Wisconsin, Madison, Wisconsin, USA.

²NASA Jet Propulsion Laboratory, Pasadena, California, USA.

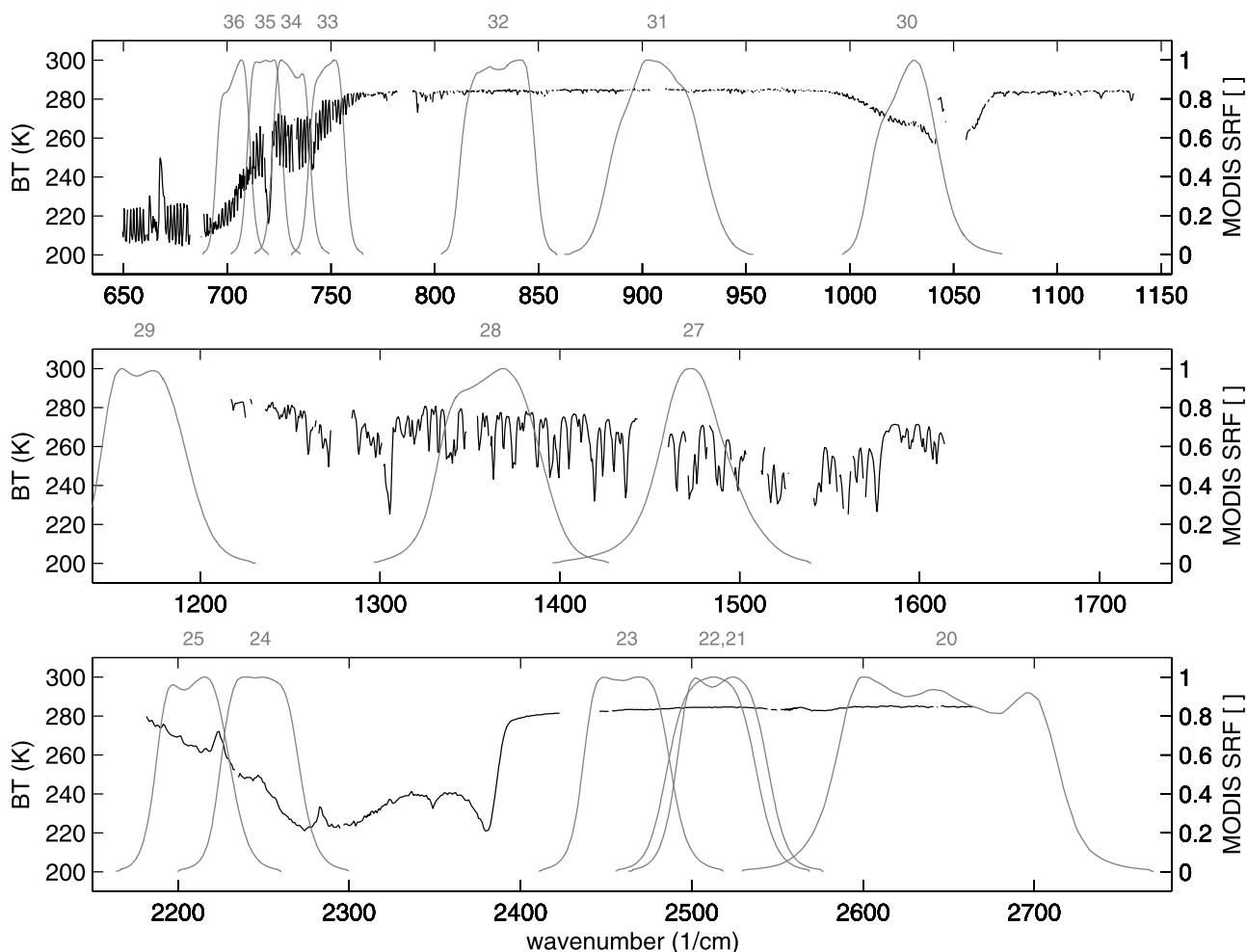


Figure 1. A sample AIRS brightness temperature spectrum (solid curve) collected on 18 February 2004 at ~0630 UTC off the east coast of Florida with the detector averaged Aqua MODIS SRFs (shaded curves) overlaid. The MODIS spectral band numbers are noted along the top of each panel.

MODIS [e.g., Moeller *et al.*, 2003a, 2003b; Xiong *et al.*, 2003; Wan *et al.*, 2004] radiances. On the basis of these studies and the inherent advantages offered by high spectral resolution for radiometric [Goody and Haskins, 1998] and spectral calibration, we believe that the high-spectral resolution AIRS should be considered the primary standard when comparing AIRS and MODIS radiances. However, rather than focus on the assessment of the absolute accuracy of either sensor, the primary purpose of this paper is to provide a characterization of the differences between the AIRS and MODIS observed radiances. This is important for various climate related studies which rely on the accuracy of the sensors, for understanding biases between AIRS Level 2 products and MODIS Level 2 products, and for development of applications that utilize radiance data from both AIRS and MODIS. Relevant examples of the latter are recent AIRS cloud-clearing studies incorporating infrared MODIS data [Huang and Smith, 2004; Goldberg *et al.*, 2004; Smith *et al.*, 2004; Li *et al.*, 2005b] and the synergistic use of AIRS and MODIS for cloud property retrievals [Li *et al.*, 2004a, 2004b, 2005a]. Demonstration of a technique for creating precise and accurate comparisons of a high-spectral resolution

sensor with a broadband sensor is also important considering the next generation of high-spectral resolution infrared observations from geostationary orbit, which have the potential to be used as a reference for accurately intercomparing all polar orbiting sensors.

[4] The remainder of this paper presents a detailed comparison of AIRS and MODIS infrared radiances collected on 6 September 2002 and 18 February 2004. Section 2 is a description of the analysis techniques. Section 3 describes what data are used. Section 4 presents the AIRS-MODIS differences with a discussion of the analysis and results, and section 5 is a summary.

2. Data Analysis

[5] With both AIRS and MODIS mounted on the same polar orbiting platform, making measurements at the same view angles that are collocated very well in space and time, the process of intercomparing AIRS and MODIS radiances is relatively straightforward. It involves reducing the high-spectral resolution AIRS spectra to match the MODIS band spectral responses and reducing the high-spatial resolution MODIS data to lower spatial resolution suitable for com-

Table 1. Summary of Mean AIRS Minus MODIS Brightness Temperature Differences

MODIS Band Number	CWL (Bandwidth), ^a μm	6 September 2002				18 February 2004						
		Mean AIRS BT, K	CC (Range), ^b K	Mean Difference (Uncertainty), K	Standard Deviation Difference, K	Mean AIRS BT, K	CC (Range), ^b K	Mean Difference (Uncertainty), K	Standard Deviation Difference, K	Change (Uncertainty), ^d K		
21	3.98 (3.94–4.02)	297.0	0.01 (0.00)	0.09 (0.00)	0.23	187,487	298.4	0.01 (0.00)	-0.33 (0.00)	0.18	80,388	0.42 (0.00)
22	3.97 (3.93–4.02)	286.8	0.00 (0.00)	-0.08 (0.00)	0.84	211,056	284.5	0.00 (0.00)	-0.14 (0.00)	0.25	246,112	-0.06 (0.00)
23	4.06 (4.02–4.11)	284.3	-0.19 (0.16)	0.14 (0.08)	0.17	244,064	283.3	-0.19 (0.16)	0.04 (0.08)	0.20	277,755	-0.10 (0.08)
24	4.45 (4.40–4.50)	243.4	0.00 (0.03)	-0.22 (0.02)	0.24	559,547	243.0	0.08 (0.04)	-0.30 (0.02)	0.25	511,821	-0.07 (0.02)
25	4.53 (4.48–4.57)	259.2	-0.25 (0.16)	0.03 (0.08)	0.13	453,068	255.4	-0.38 (0.21)	-0.03 (0.11)	0.18	73,261	-0.07 (0.09)
27	6.78 (6.69–6.88)	245.9	0.57 (0.21)	1.05 (0.11)	0.30	1,044,122	242.8	0.57 (0.21)	0.67 (0.11)	0.39	1,098,476	-0.38 (0.11)
28	7.35 (7.19–7.51)	256.9	-0.67 (0.37)	0.48 (0.19)	0.25	1,149,593	254.8	-0.67 (0.37)	0.38 (0.19)	0.21	1,250,087	-0.09 (0.19)
30	9.73 (9.58–9.89)	249.1	0.93 (0.24)	-0.41 (0.12)	0.26	172,064	249.1	0.91 (0.25)	-0.70 (0.13)	0.23	358,698	-0.29 (0.13)
31	11.02 (10.76–11.30)	275.0	0.13 (0.04)	0.03 (0.02)	0.12	322,522	273.2	0.13 (0.05)	0.06 (0.03)	0.09	393,559	0.03 (0.03)
32	12.04 (11.78–12.31)	275.1	0.00 (0.05)	0.10 (0.03)	0.16	330,994	272.5	-0.01 (0.02)	0.12 (0.01)	0.13	401,780	0.02 (0.02)
33	13.37 (13.21–13.52)	259.7	-0.28 (0.22)	0.07 (0.11)	0.21	716,940	257.6	-0.21 (0.16)	0.06 (0.08)	0.16	817,442	-0.01 (0.10)
34	13.68 (13.51–13.86)	249.2	0.11 (0.04)	-0.34 (0.02)	0.15	1,089,663	247.9	0.49 (0.23)	-0.48 (0.12)	0.12	1,228,199	-0.14 (0.07)
35	13.92 (13.76–14.09)	240.5	-0.21 (0.09)	-0.57 (0.05)	0.28	1,318,406	240.0	-0.17 (0.07)	-0.55 (0.04)	0.31	1,480,551	0.02 (0.05)
36	14.22 (14.06–14.39)	226.1	-0.12 (0.11)	-0.88 (0.06)	0.43	1,980,369	226.9	-0.12 (0.11)	-0.81 (0.06)	0.51	2,151,789	0.07 (0.06)

^aCenter wavelength and bandwidth of the MODIS band.^bMean and range of convolution correction.^cNumber of uniform fields of view, out of a possible total of 2,916,000.^dDifference between 6 September 2002 and 18 February 2004 mean differences.

parison to AIRS. These steps are described in sections 2.1 and 2.2 respectively. The third aspect of this analysis is the selection of spatially uniform scenes, also presented in section 2.2. As described further in section 4, the selection of uniform scenes excludes radiometric differences associated with spatially nonuniform scenes from this characterization study, but greatly simplifies the intercomparison process, particularly with respect to precise representation of the AIRS and MODIS geolocated footprints.

2.1. Reducing AIRS Spectra to MODIS Spectral Resolution

[6] AIRS radiance spectra are reduced to match the MODIS spectral responses by convolving the AIRS spectra with the MODIS SRF for each MODIS band. If the AIRS spectra were of infinite spectral resolution and contained no spectral gaps within the MODIS spectral bands, then this approach would be exact. However, small gaps present in the AIRS spectral coverage require that corrections (referred to herein as “convolution corrections,” or CC) be applied to these convolved values. The corrections are computed by simulating the effects of the AIRS spectral gaps in computed spectra for each MODIS band, and are given by:

$$CC = R_{\text{MONO}} \otimes \text{SRF}_{\text{MODIS}} - (R_{\text{MONO}} \otimes \text{SRF}_{\text{AIRS}}) \otimes \text{SRF}_{\text{MODIS}} \quad (1)$$

where R_{MONO} is a monochromatic spectrum of upwelling earth scene radiance at 705 km, $\text{SRF}_{\text{MODIS}}$ are the MODIS SRFs, SRF_{AIRS} are the AIRS SRFs, and \otimes denotes a spectral convolution. In this equation, $R_{\text{MONO}} \otimes \text{SRF}_{\text{MODIS}}$ simulates the radiance observed by MODIS while $(R_{\text{MONO}} \otimes \text{SRF}_{\text{AIRS}}) \otimes \text{SRF}_{\text{MODIS}}$ simulates the radiance computed when convolving an AIRS spectrum with the MODIS SRFs, as done in this analysis when comparing AIRS and MODIS. When an actual observed AIRS radiance spectrum (R_{AIRS}) is convolved with the MODIS SRFs, the correction is therefore included to account for the simulated differences (i.e., $R'_{\text{AIRS}} = R_{\text{AIRS}} \otimes \text{SRF}_{\text{MODIS}} + CC$). To ensure that the AIRS spectral gaps are treated consistently, it is necessary that the same set of AIRS channels used in the actual observed spectra also be used when evaluating equation (1). Selection of AIRS channels is presented in section 3. CC is dependent on the atmospheric state, surface, and cloud conditions used in the simulation of R_{MONO} . The values of CC used in this data analysis are the mean of those computed for each of the six standard atmospheres [McClatchey *et al.*, 1972] via clear sky simulations using the kCARTA line-by-line algorithm [Strow *et al.*, 2003a], shown in Figure 2. The uncertainty of the convolution corrections is proportional to the variability of CC as a function of atmospheric state, and therefore an estimate of this variability is carried as an uncertainty in the resulting comparisons. The mean values of CC and the range of CC for the standard atmospheres are listed in columns 4 and 9 of Table 1 for 6 September 2002 and 18 February 2003 respectively. Large spectral gaps are present in the AIRS spectra within MODIS bands 20 and 29 and AIRS-MODIS comparisons are therefore not performed for those bands. Significant gaps are also present within MODIS bands 25, 27, 28, 30, and 34 resulting in the largest mean values of CC. Band 27 (7.3 μm , typically sensitive to midlevel and lower-level temperature and water vapor) has

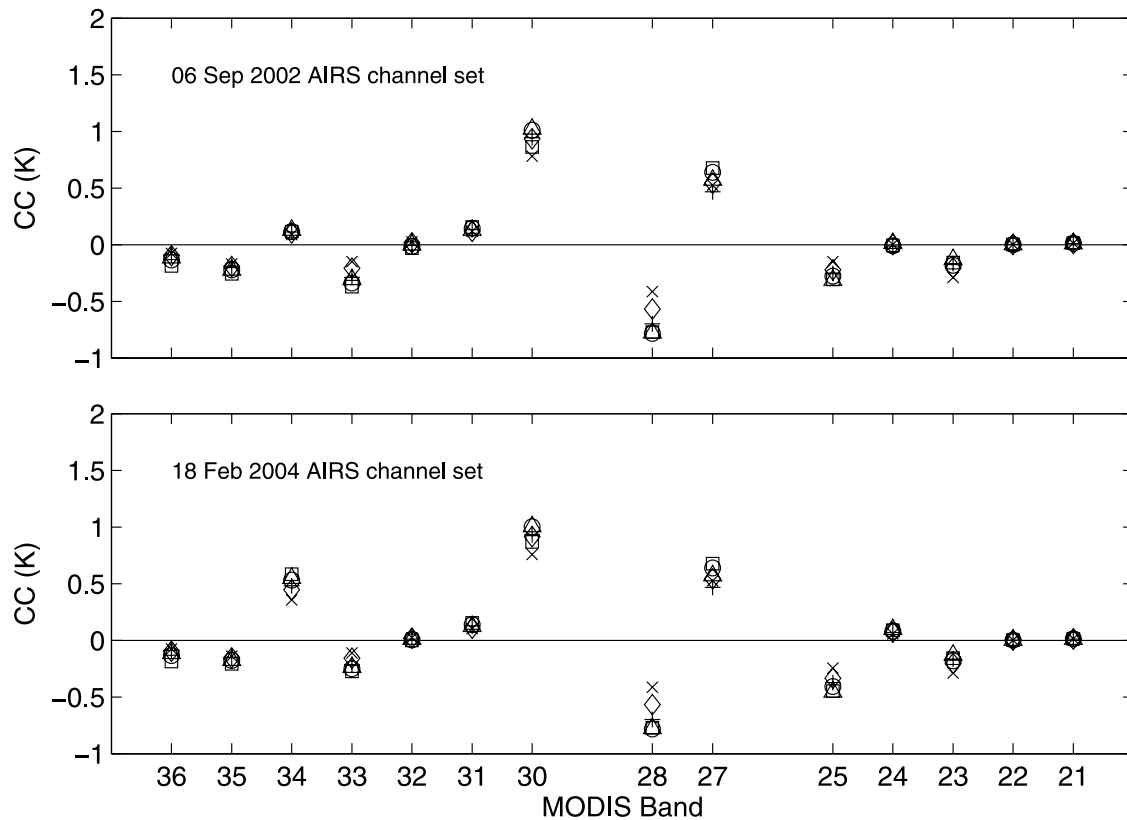


Figure 2. Convolution corrections computed for the AIRS channel sets used for the (top) 6 September 2002 and (bottom) 18 February 2004 data processing for the six standard atmospheres (squares indicate tropical, circles indicate midlatitude summer, diamonds indicate midlatitude winter, pluses indicate subarctic summer, crosses indicate subarctic winter, and asterisks indicate U.S. Standard).

the largest dependence of CC on atmospheric state. Further discussion of the uncertainties associated with the convolution corrections is included in section 4.

[7] The AIRS-MODIS comparisons are presented in terms of equivalent brightness temperature rather than radiance. From both the polychromatic observed MODIS radiances and from R'_{AIRS} , brightness temperatures (BT_{AIRS} , BT_{MODIS}) are computed using the Planck function supplemented with linear monochromaticity correction coefficients [Weinreb *et al.*, 1997] computed for the Aqua MODIS bands.

2.2. Spatial Collocation of MODIS and AIRS and Selection of Uniform Scenes

[8] For each AIRS FOV, the 1 km resolution MODIS data are degraded to lower spatial resolution by (1) representing the AIRS geolocated footprint as an oversized circular footprint, (2) determining MODIS pixels that are geolocated within the AIRS footprint, and (3) computing the mean of these MODIS radiances for each MODIS band (R_{MODIS}). The standard deviation of the MODIS data within each AIRS footprint is also computed and retained for selection of spatially uniform scenes.

[9] The actual AIRS instantaneous angular FOV is $1.1 \times 0.6^\circ$. Assuming a circular FOV of 1.1° yields a geolocated nadir footprint 13.5 km in diameter. For off nadir scan angles these footprints become elliptical, and at the maximum scan angle of 49.5° the major (cross track) and minor

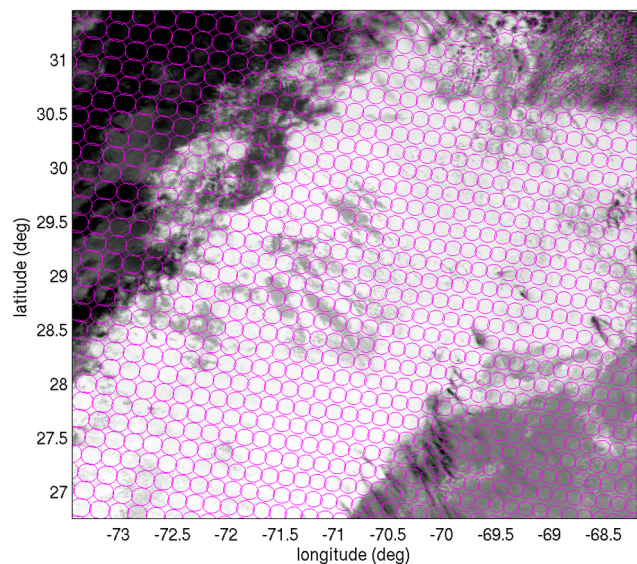


Figure 3. MODIS band 31 ($11 \mu\text{m}$) brightness temperatures (collected on 18 February 2004 at ~ 0630 UTC off the east coast of southern Florida) overlaid with approximate representations of the AIRS footprints (magenta circles) used in the collocation process. The MODIS brightness temperatures are displayed with a gray color scale going linearly from 255 (black) to 295 K (white).

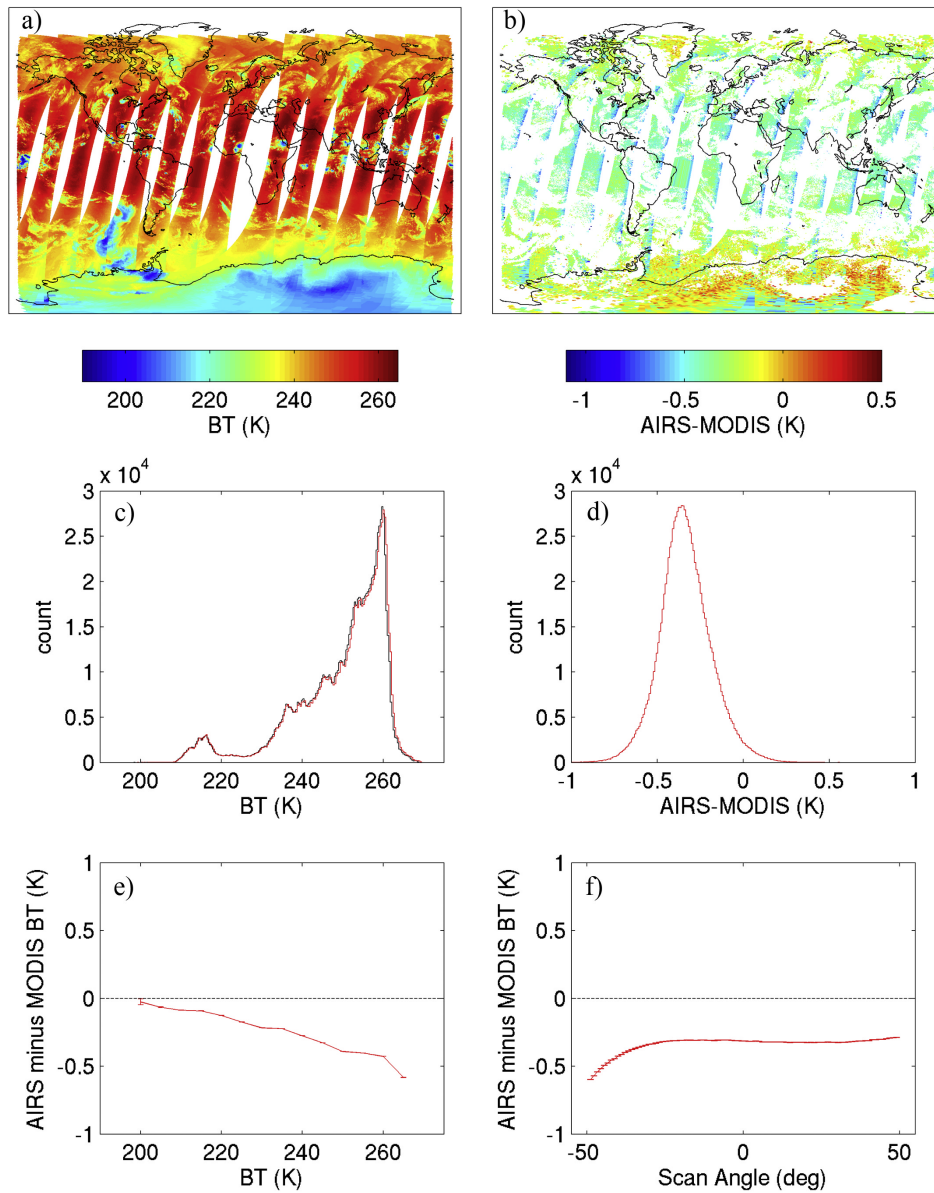


Figure 4. Brightness temperature comparisons for MODIS band 34 ($13.7 \mu\text{m}$) on 6 September 2002, including images of the descending (nighttime) (a) MODIS observed brightness temperatures and (b) brightness temperature differences (AIRS minus MODIS) for the selected uniform scenes, (c) histograms of the AIRS and MODIS observations, (d) a histogram of the brightness temperature differences, (e) the differences as a function of scene temperature, and (f) the differences as a function of scan angle. Vertical error bars in Figures 4e and 4f are the uncertainty in the mean for each bin.

(along track) axes are approximately 21 and 33 km respectively. For this application, the AIRS footprints are represented as circles with diameter increasing from 14.85 km (10% larger than 13.5) at nadir to 36.3 km (10% larger than 33) at 49.5° off nadir. This is illustrated in Figure 3, which is an image of MODIS band 31 ($11 \mu\text{m}$) brightness temperatures collected on 18 February 2004 at ~ 1629 UTC off the east coast of Florida overlaid with approximate AIRS footprints. Representing the footprints as circles leads to a significant computational efficiency when collocating the MODIS data. When determining which MODIS data are geolocated within the AIRS footprints, the MODIS foot-

prints are assumed to be of infinite spatial resolution with positions given in the 1 km geolocation files (i.e., fractional MODIS footprints on the edges of the AIRS footprints are not considered). Because of the scan patterns of both AIRS and MODIS, the number of collocated MODIS pixels varies with scan angle, increasing from roughly 170 for nadir AIRS footprints to over 320 at 49.5° off nadir.

[10] Combined with a scheme to select spatially uniform scenes, this efficient and approximate method for representing the AIRS FOVs as oversized circles is adequate for collocating the AIRS and MODIS data; by selecting spatially flat fields, the comparisons are not sensitive to the

approximations introduced here. Spatially uniform footprints are selected by requiring that the standard deviation of the MODIS scene brightness temperatures within the AIRS footprints is less than a threshold value. The threshold is 0.2 K for all bands with the exception of fire detection band 21 which has a threshold of 1.0 K because of its higher noise level. With the exception of yield, there are no significant changes in the results presented in section 4 if these thresholds are increased by a factor of 2, implying that this spatial collocation approach is appropriate. The scene selection is done independently for each MODIS band, resulting in more retained footprints for bands which sense higher in the atmosphere. This selection also does not necessarily exclude cloudy scenes or scenes over land. Images of the selected uniform footprints are shown in section 4 and the total number of uniform footprints are listed in columns 7 and 12 of Table 1.

3. Data

[11] This section describes the version of various data, SRF, and other files used in this study. The MODIS L1B radiance and 1 km geolocation data are “collection 3” processing for 6 September 2002 (e.g., MYD021K-M.A2002249.1815.003.2002251013129.hdf) and “collection 4” for 18 February 2004 (e.g., MYD021KM.A2004049.1850.004.2004050195816.hdf). AIRS L1B processing is version 2.6.7 (e.g., AIRS.2002.09.06.026.L1B.AIRS_Rad.v2.6.7.3.A02249222409) for 6 September 2002 and version 3.0.10 (e.g., AIRS.2004.02.18.027.L1B.AIRS_Rad.v3.0.10.G04049222941.hdf) for 18 February 2004. For the comparisons presented here, which are averages over many spatially uniform scenes, the differences between collections 3 and 4 processing for MODIS, and between L1B versions v2.6.7 and v3.0.10 for AIRS, are negligible. For example, maximum differences of ~ 5 mK were found when comparing collection 3 and collection 4 MODIS band 36 brightness temperatures for 6 September 2002.

[12] Not all of the 2378 AIRS spectral channels are included in the analysis. Using AIRS channel properties files provided by the AIRS team, channels that are not recommended for use in Level 2 processing are excluded (using the “L2_Ignore” flag). These channels have unusually high noise levels, exhibit a non-Gaussian noise behavior called “popping,” have SRF centroids or shapes which do not match the AIRS sensor model, and/or have spatial centroids which are more than 0.25° from the nominal boresight. Different channel properties files are assigned for use for different time periods throughout the AIRS mission. For 6 September 2002, the L2.chan_prop.2002.10.22.v6.6.4.anc file is used and 2096 channels are retained. For 18 February 2004, L2.chan_prop.2003.11.19.v8.1.0.anc is used and 2102 channels are retained. (For 18 February 2004, in addition to the channels excluded on the basis of the channel properties file, another eleven channels

were also found to be frequently out of range and are also excluded). The convolution corrections (equation (1)) are evaluated separately using these two channel sets, as shown in Figure 2, and used for the 6 September 2002 and 18 February 2004 comparisons respectively. Note that with the convolution correction treatment used here, it is necessary to use the same channel set for all spectra on a given day; otherwise CC would be required to be updated as useful channels are selected on a FOV by FOV or granule by granule basis.

[13] The AIRS SRFs used in evaluating equation (1) are provided by the AIRS team and given in the file “srftables_m135_fringes.hdf.” These SRFs are computed with a sensor model for the on-orbit grating temperature of 155.13 K, a grating/detector focal plane offset of -13.5 microns, and filter window temperature of 156.16 K [Strow *et al.*, 2003b]. AIRS SRF data files are available online at <http://asl.umbc.edu/pub/airs/srf/srfhdf.html> and http://www.ssec.wisc.edu/~paulv/Fortran90/Instrument_Information/SRF/Data_Files.html.

[14] The MODIS SRFs used in equation (1) are linear averages of the ten individual detector SRFs. The individual detector SRFs are provided by the MODIS Calibration Support Team and are available online at <ftp://ftp.mcst.sai.biz/pub/permanent/MCST/>. The detector averaged SRFs are the same SRFs used in the production of MODIS Level 2 atmosphere and cloud products. These SRFs are contained in the file `modis_aqua.srf.nc` which is available online at http://www.ssec.wisc.edu/~paulv/Fortran90/Instrument_Information/SRF/Data_Files.html. Note that although there is little variability among the individual detector’s SRFs for a given band, the use of detector averaged SRFs is consistent with the MODIS spatial averages described in section 2.2, which include contributions from all ten detectors.

4. Results and Discussion

[15] Following the data analysis techniques presented in section 2 and using the data described in section 3, the resulting AIRS-MODIS comparisons are presented and discussed here. Example comparisons for MODIS band 34 ($13.7 \mu\text{m}$) are shown in Figure 4, which includes images of the MODIS observed brightness temperatures and AIRS-MODIS brightness temperature differences, histograms of the AIRS and MODIS brightness temperatures and brightness temperature differences, and plots of the differences as a function of scene temperature and scan (view) angle. Figures 5–10 contain similar images and plots (and also differences plotted as a function of solar zenith angle), but for all of the MODIS bands. Table 1 lists various parameters summarizing the mean brightness temperature comparisons including, for each band, the mean observed brightness temperature, mean and range of the convolution correction, ensemble mean and standard deviation of the brightness temperature differences, number of selected uniform footprints, and the change in mean brightness temperature

Figure 5. Descending (nighttime) (left) MODIS brightness temperatures and (right) AIRS minus MODIS brightness temperature differences on 6 September 2002 for MODIS bands 36 through 30. The left hand tick marks of the color scale apply to the MODIS brightness temperature images, and the right hand tick marks apply to the brightness temperature difference images.

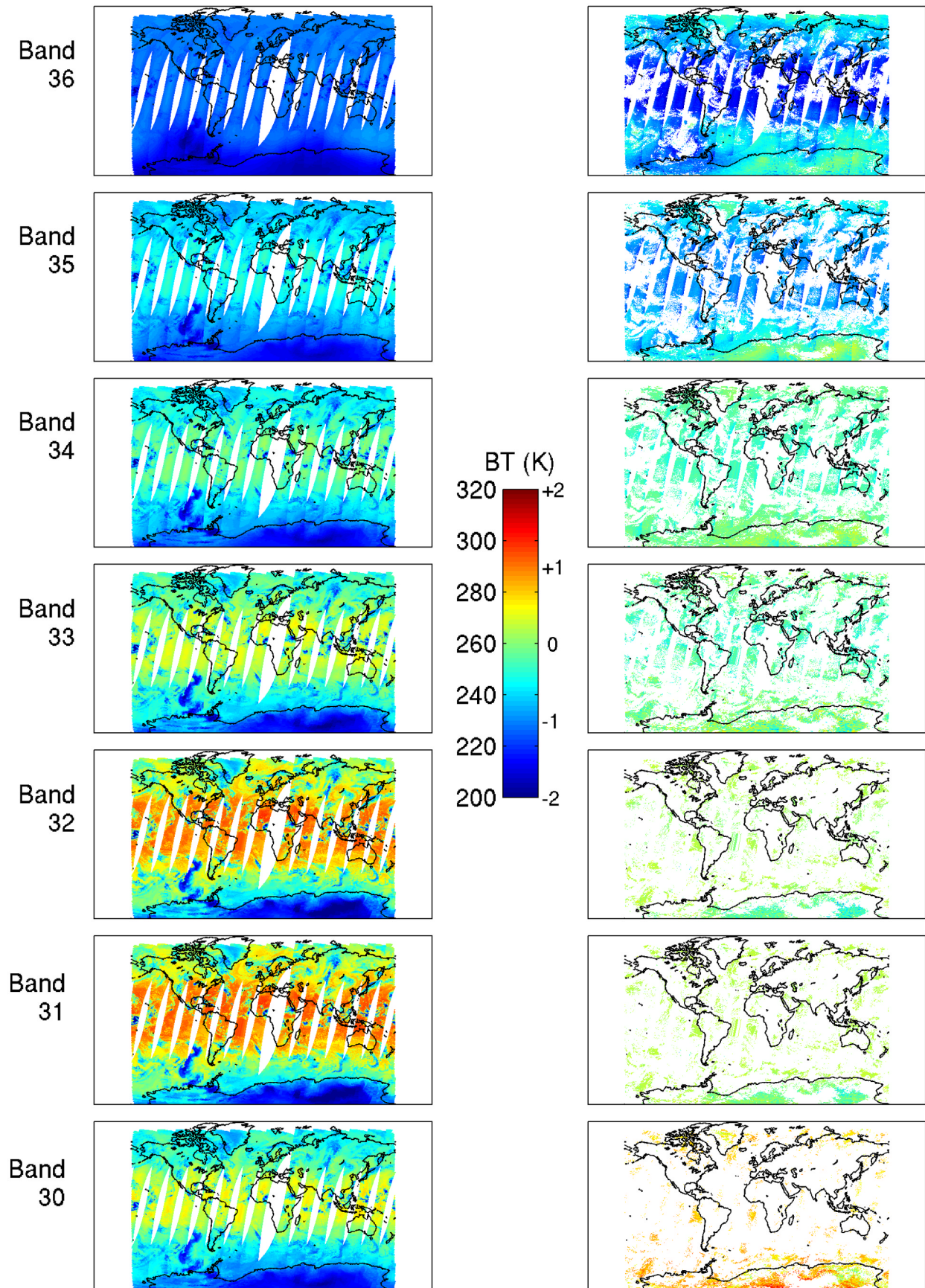


Figure 5

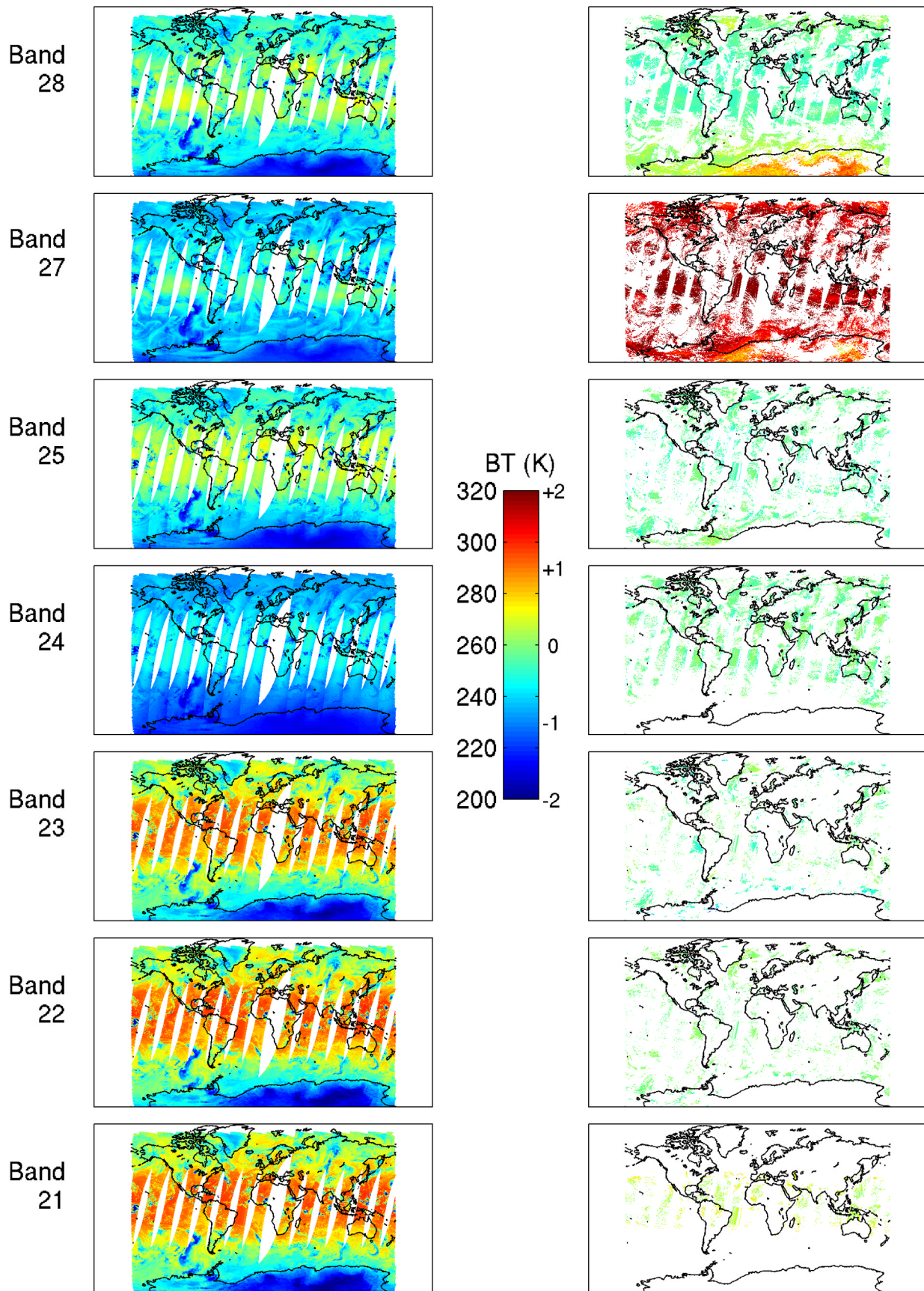


Figure 6. Same as Figure 5 but for MODIS bands 28 through 21.

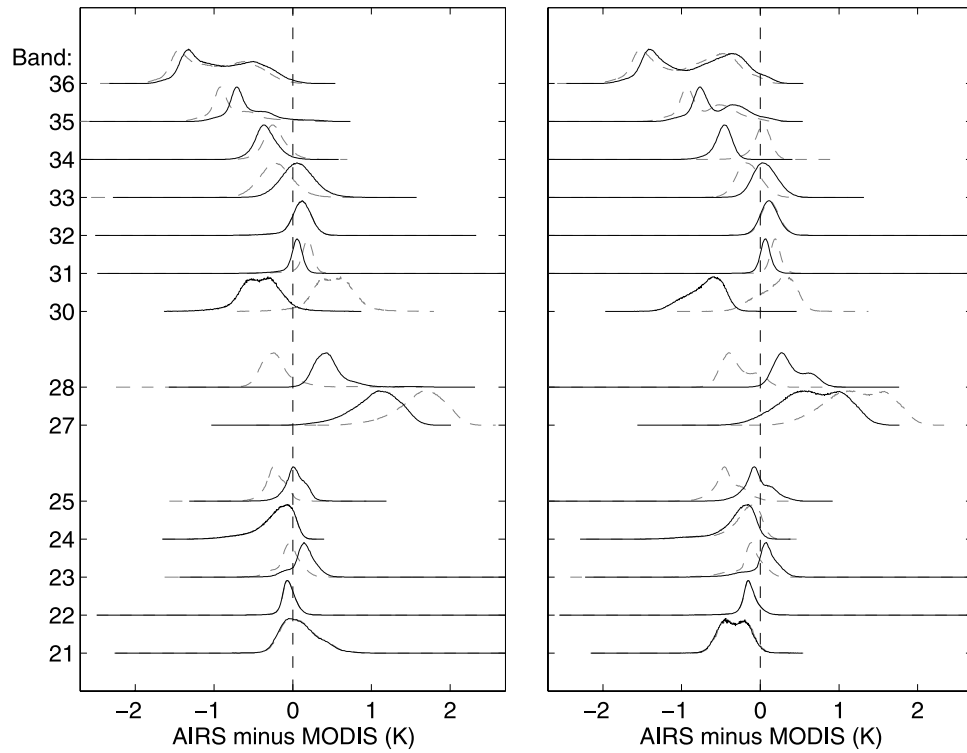


Figure 7. Histograms of AIRS minus MODIS brightness temperature differences for each band for (left) 6 September 2002 and (right) 18 February 2004. Distributions of differences computed without the convolution corrections are included (the dashed shaded curves) to illustrate the size of the corrections.

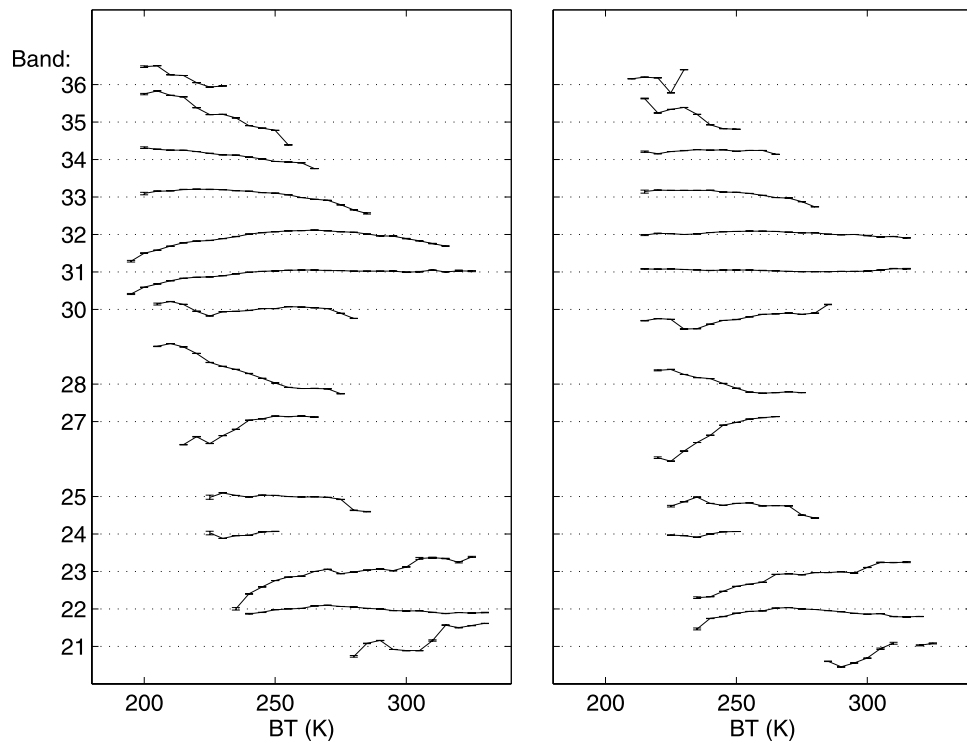


Figure 8. AIRS minus MODIS brightness temperature differences presented as a function of scene brightness temperature for each band for (left) 6 September 2002 and (right) 18 February 2004. For each band, the horizontal grid lines denote 0 K (e.g., each curve is offset in the vertical), and each vertical tick mark represents a change of 1 K. The mean AIRS minus MODIS difference (for all scene temperatures) is subtracted from the plotted values. Means are computed for 5 K scene temperature bins, and the vertical error bars are the uncertainty in the mean for each bin.

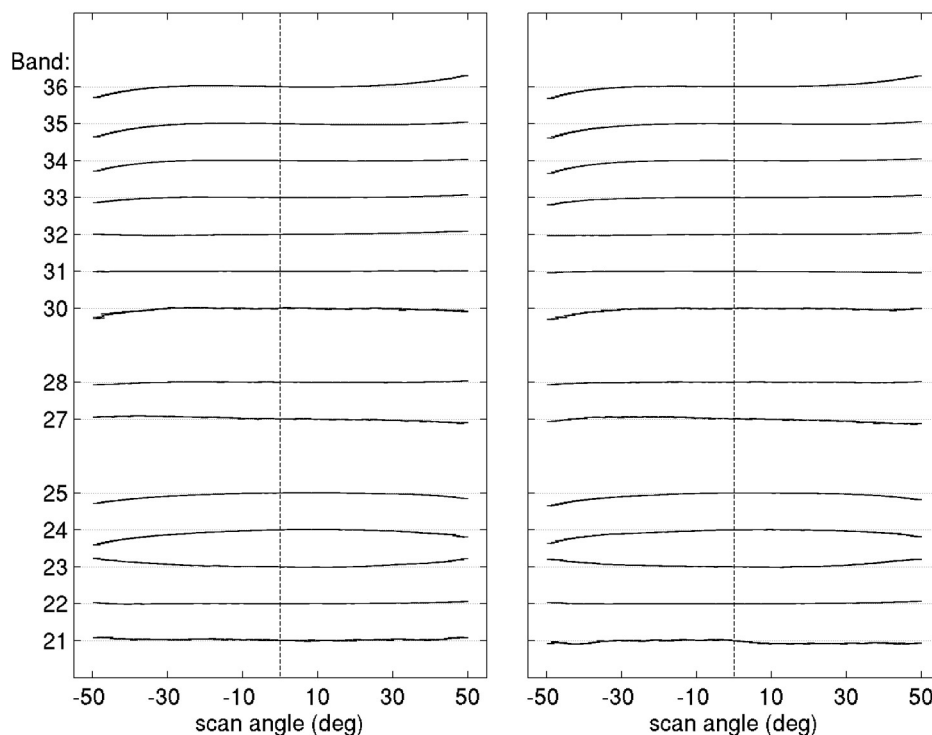


Figure 9. AIRS minus MODIS brightness temperature differences presented as a function of scan (view) angle for each band for (left) 6 September 2002 and (right) 18 February 2004. For each band, the horizontal grid lines denote 0 K (e.g., each curve is offset in the vertical), and each vertical tick mark represents a change of 1 K. The AIRS minus MODIS difference at nadir is subtracted from the plotted values. Means are computed for the 90 AIRS scan angles, and the vertical error bars are the uncertainty in the mean for each angle.

differences from 6 September 2002 to 18 February 2004. The overall mean brightness temperature differences are also plotted in Figure 11.

[16] The comparisons shown in Figure 4 for band 34 on 6 September 2002 demonstrate the statistical robustness and straightforwardness of this analysis. Uniform scenes are selected over ocean, land (including desert), polar regions, and clouds. With over 1.3 million footprints covering a wide range of conditions included in this comparison, dependencies of the differences as a function of scene temperature, scan angle, and solar zenith angle are clearly defined. Vertical error bars in each of the plots are uncertainties in the mean values. The comparisons for band 34 show a mean brightness temperature difference of -0.34 K (MODIS warmer than AIRS) with the differences decreasing from ~ 0 K for scene temperatures of 200 K to -0.6 K for scene temperatures of ~ 270 K. The differences also have a clear dependence on scan angle for scan angles between -30 and -50° (at end of scan for MODIS). The remainder of this section includes more detailed discussion of the comparisons for all of the bands and a discussion of the absolute uncertainties of the comparisons.

[17] When considering sources of absolute error associated with the determination of the AIRS-MODIS differences presented here, the limiting uncertainty is associated with the convolution corrections. The only other contributors are collocation related errors, which are considered to be negligible (random with zero mean) given the large

number of resulting footprints included in the comparisons. Bands for which the variation of the convolution correction with atmospheric state is large (e.g., band 28) have larger uncertainty. This results from using the mean convolution correction (of values computed over the six standard atmospheres) for all scenes. Absolute uncertainties in the AIRS-MODIS brightness temperature differences are estimated as half the full range of the convolution corrections over the six atmospheres. When computing the uncertainty of the change in the mean differences between 6 September 2002 and 18 February 2004 (column 13 of Table 1), the uncertainties are not additive since the variability of the AIRS spectra are very similar on both days (i.e., the same systematic error is present in both differences) and the uncertainty in the changes are computed as the mean of uncertainties from both days. These are thought to be conservative (high) estimates, since the variability of the correction is largest for clear sky scenes. Note that for bands 34 and 23 the use of the convolution corrections actually increases the size of the AIRS-MODIS differences. Consider band 34, however, which used significantly different AIRS channel sets on 6 September 2002 and 18 February 2004. The resulting convolution corrections are significantly different on the 2 days (0.11 K versus 0.49 K); however, the final comparisons in Figure 7 for these 2 days are very similar, empirically giving confidence in the approach. A more accurate but significantly more computationally expensive treatment of the convolution correction, to be

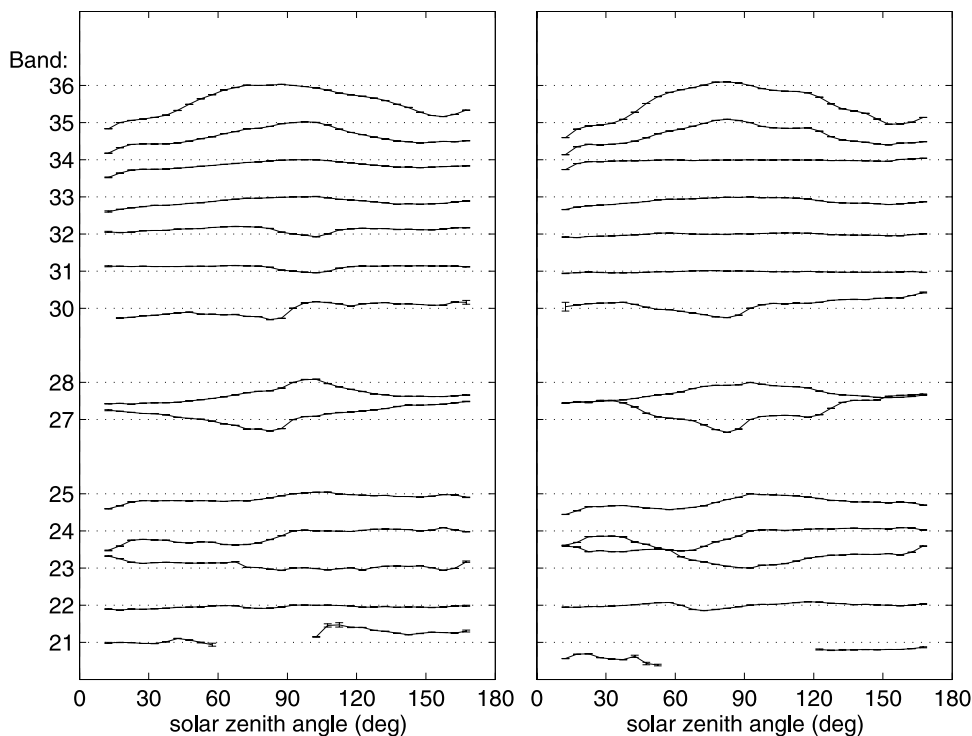


Figure 10. AIRS minus MODIS brightness temperature differences presented as a function of solar zenith angle for each band for (left) 6 September 2002 and (right) 18 February 2004. For each band, the horizontal grid lines denote 0 K (e.g., each curve is offset in the vertical), and each vertical tick mark represents a change of 1 K. The AIRS minus MODIS difference for solar zenith angle of 90° is subtracted from the plotted values. Means are computed for 5° angle bins and the vertical error bars are the uncertainty in the mean for each bin.

considered in future investigation, involves calculation of the corrections independently for each field of view (i.e., requiring knowledge of the surface, clouds, and atmospheric state for calculation of R_{MONO} via direct calculation or regression).

[18] Since only spatially uniform scenes are used in the comparisons presented here, the comparisons are not sensitive to geolocation errors, including characterization of the spatial response functions of either sensor. The comparisons also do not characterize any type of radiometric errors associated with nonuniform scenes. The AIRS project at

the Jet Propulsion Laboratory is developing a set of AIRS spatial response functions for all scan angles that are required to coregister MODIS and AIRS data in nonuniform scenes.

[19] Mean values of the AIRS-MODIS differences for all bands can be seen in Figures 7 and 11 and are also listed in Table 1. Taking the uncertainty estimates into account, agreement of 0.1 K or better is found for bands 21, 22, 23, 25, 31, 32, and 33 on 6 September 2002 and for bands 23, 25, 31, and 33 on 18 February 2004. Mean differences for ozone sensitive band 30 are -0.4 ± 0.1 K and $-0.7 \pm$

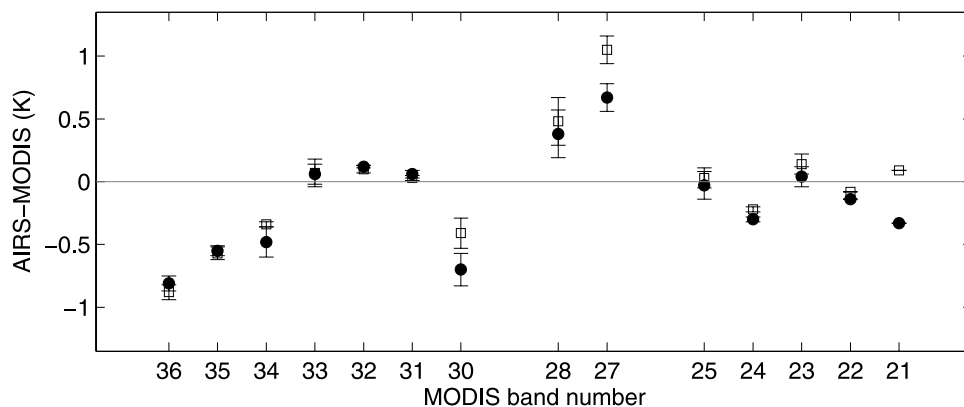


Figure 11. Mean AIRS minus MODIS brightness temperature differences and uncertainties for 6 September 2002 (open squares) and 18 February 2004 (solid circles).

0.1 K (MODIS warmer than AIRS) on the 2 days. As discussed further below, differences for water vapor bands 27 and 28 and temperature sounding bands 34, 35, and 36 exhibit a clear dependence on scene temperature. Combined with bipolar distributions of the scene temperatures, this produces difference distributions that also become bipolar, as seen in Figure 7. The differences for longwave temperature sounding bands grow from near zero for band 33 to over -1 K for band 36 (MODIS warmer than AIRS). Differences for water vapor bands 27 and 28 exceed 0.5 K on both days (AIRS warmer than MODIS).

[20] Periodic validations of AIRS spectral radiances with underflights by the airborne Scanning High-resolution Interferometer Sounder (Scanning-HIS) [Tobin *et al.*, 2006] have shown AIRS to be accurate to better than ~ 0.2 K throughout the infrared spectrum. In addition, assessments of Aqua (and Terra) MODIS calibration by Moeller *et al.* [2003a, 2003b] have shown differences for the longwave CO₂ bands 35 and 36 which are similar to those reported here. These findings suggest that the significant AIRS-MODIS differences observed here for longwave CO₂ bands 34, 35, and 36 should be attributed to MODIS. Furthermore, as presented below, the mean differences and the scene temperature dependence of these differences can be nearly eliminated by introducing spectral shifts for the MODIS SRFs for these bands.

[21] Taking the uncertainty estimates into account, changes in the mean brightness temperature differences from 6 September 2002 and 18 February 2004 are found to be 0.1 K or less for all bands with the exception of three bands. As discussed later, the dependencies on scene temperature, scan angle, and solar zenith angle are also very similar for the 2 days. This suggests that, at least to first order, time-independent biases can be used to account for the differences between AIRS and MODIS for these bands. For bands 21, 27, and 30, the changes are 0.42 ± 0.00 K, -0.38 ± 0.11 K, and -0.29 ± 0.13 K, respectively. For band 27, small changes in the mean scene temperature between the 2 days, combined with the signal level dependence of the differences, may account for some of the change observed for this band. A known dependence of the band 27 SRF on the intermediate stage window temperature is probably contributing to the change in bias from 3 September 2002 to 18 February 2004. Aqua MODIS telemetry shows that the window temperature has risen by about 2 K between these dates, and the band 27 linear gain term (b_1) has decreased by 1–2%. If the b_1 decrease is assigned entirely to SRF change, it would result in about a 0.5 K offset in the MODIS band 27 calibrated radiances. The change in the band 21 (fire band) results is largely due to updates in the MODIS band 21 gain term of the calibration, which is evaluated quarterly using the special OBC-BB warm-up and cool-down mode of operation. The band 21 gain term was changed twice (11 September 2002 and 31 July 2003) between 6 September 2002 and 18 February 2004. Future work in this area involves extending these comparisons to include 1 day per season (e.g., winter and summer solstice, spring and fall equinox) and tracking the changes (or lack thereof) over the entire Aqua mission.

[22] The AIRS-MODIS differences are presented as a function of scene temperature in Figure 8. Even for bands that sense the lower atmosphere and surface, a large number

of uniform footprints are selected, covering a wide range of typical scene temperatures. The scene temperature dependence of the differences is similar on both days; an exception is for band 36 which displays a clear dependence on scene temperature on 6 September 2002, but not as clear on 18 February 2004. As mentioned previously, significant dependence of the AIRS-MODIS differences on scene temperature can be seen for bands 27, 28, 34, 35, and 36, and to some extent also for bands 23 and 33. Although the convolution corrections vary in size with changes in the atmospheric state, this is not considered to be an interpretation issue given the relative size of the observed scene dependence and size and variability of the convolution corrections. For example, consider band 35 for which the AIRS-MODIS differences vary by over 1 K for scene temperatures ranging from 200 to 260 K while the convolution corrections have a range of less than 0.1 K for a wide range of atmospheres. These observed differences are also found to increase linearly with contrast to the window region brightness temperature (i.e., for band 35, $BT_{\text{AIRS},35} - BT_{\text{MODIS},35}$ increases linearly with $BT_{\text{MODIS},35} - BT_{\text{MODIS},31}$), which can be indicative of an uncharacterized radiometric nonlinearity or possibly an indication of an error in the knowledge of the MODIS SRF positions. AIRS can resolve individual absorption lines and its spectral calibration is known with high absolute accuracy [Strow *et al.*, 2003b]. Investigation of the spectral shift hypothesis is presented in Figure 12, where a small shift in the MODIS SRF position is introduced for band 35. For one orbit of data, instead of convolving the AIRS spectra with the nominal MODIS SRF, the convolutions are performed with the SRF shifted by $+0.8$ cm⁻¹ (15.5 nm). This value was determined by iteration and finding the shift which provides best agreement with AIRS. Differences without the shift clearly show a scene temperature dependence and a bimodal distribution, with a mean value of -0.55 ± 0.28 K. Introducing the shift removes the scene temperature dependence of the differences almost completely, tightens the distribution, and reduces the mean difference to $+0.07 \pm 0.09$ K. Similar improvements are found for bands 27, 28, 34, and 36 using shifts of approximately 5.0 cm⁻¹ (22.9 nm), 2.0 cm⁻¹ (10.7 nm), 0.8 cm⁻¹ (15.0 nm), and 1.0 cm⁻¹ (20.2 nm) respectively. The MODIS instrument spectral calibration was performed with the instrument in a thermal vacuum chamber and the grating spectrometer source in ambient, illuminating the MODIS through a ZnSe window. Inadequate characterization of the long-wavelength response of the ZnSe window is one possible explanation for the spectral shifts. Despite the improvements in AIRS-MODIS agreement with these shifted SRFs, it should be emphasized that this investigation is not conclusive regarding the physical source of the observed differences, and further investigation into other possible causes (e.g., radiometric nonlinearity, SRF out-of-band response) is recommended.

[23] Dependence of the AIRS-MODIS differences on scan (view) angle is shown in Figure 9. (Note that the difference at nadir for each band is subtracted from the plotted values). The observed scan angle dependencies are very similar on 6 September 2002 and 18 February 2004. Differences for bands 21, 22, 27, 28, 31, and 32 show no appreciable dependence on scan angle. Bands 24 and 25

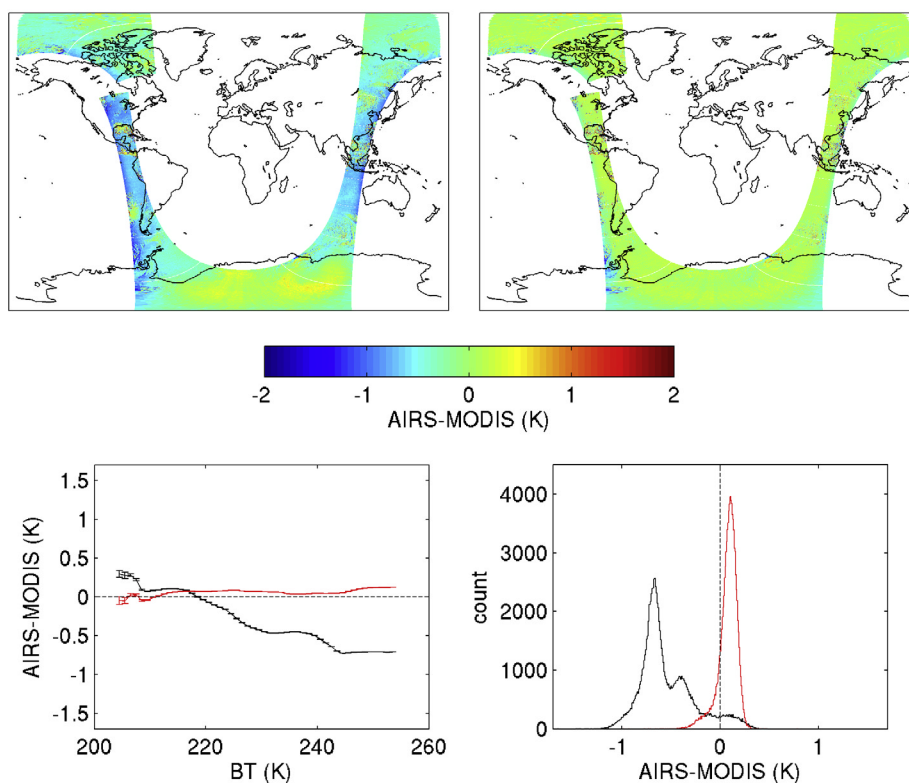


Figure 12. Band 35 ($13.9 \mu\text{m}$) brightness temperature differences using the nominal detector averaged MODIS SRF and using the SRF shifted by $+0.8 \text{ cm}^{-1}$ (15.5 nm) for one orbit on 6 September 2002. (top) Images of the brightness temperature differences (right) with and (left) without the shift, and (bottom) the scene temperature dependence and histograms of the differences with (red) and without (black) the shift.

show a highly symmetric dependence on scan angle with maximum differences of approximately -0.35 K (MODIS warmer than AIRS) at both ends of the scan (with respect to the difference at nadir). Band 23 also shows a symmetric dependence of similar magnitude but with AIRS warmer than MODIS at the ends of scan. The behavior for bands 30, 33, 34, and 35 are similar. For these bands, differences for positive scan angles have little systematic dependence on scan angle while for scan angles between -30 and -50° , the differences increase to -0.1 to -0.35 K at -49.5° off nadir (MODIS warmer than AIRS). Band 36 shows behavior similar to band 35 for negative scan angles but also has significant positive differences for positive scan angles, increasing to $+0.25 \text{ K}$ at 49.5° off nadir. As can be seen in Figure 12 (top right), it should be noted that introduction of the MODIS SRF shifts does not remove the scan angle dependence of the observed differences, as might be expected if the scan angle dependence was caused by a combination of scene temperature-dependent differences and limb darkening for larger scan angles. AIRS reported scan angles are used here; -49.5° off nadir is near the end of scan for MODIS and $+49.5$ is near the beginning of scan for MODIS. The MODIS scan mirror experiences larger angles of incidence at the end of scan relative to the beginning of scan, while AIRS utilizes a 45° mounted scan mirror and therefore has the same angle of incidence for all scan angles. Errors associated with AIRS scan angle dependence are therefore expected to be small and if present

would most likely be symmetric with scan angle, while those associated with MODIS would most likely be asymmetric with scan angle, with largest uncertainty at the end of scan. Information regarding the AIRS and MODIS polarization corrections is provided by Pagano *et al.* [2000] and Xiong *et al.* [2002, 2003] respectively. In the former paper, the AIRS scan angle dependence is verified to be calibrated to better than 0.1 K prior to launch. Using nonpolar clear sky swaths of data, the scan angle asymmetry of the AIRS and MODIS observations (rather than the dependence of the AIRS-MODIS differences on scan angle) for upper level bands 24, 33, 34, 35, and 36 has been examined. This analysis shows that the AIRS observations for all bands display scan asymmetries that are consistent with local time differences from one side of the swath to the other. For band 24, this is also true for MODIS. For the longwave bands 33–36, however, the observed MODIS scan asymmetry is nonphysical for larger scan angles. This is more pronounced for the longer wavelengths. This finding, combined with the asymmetric nature of the observed AIRS-MODIS differences versus scan angle, suggests that the scan angle dependence of the observed AIRS-MODIS differences for bands 34, 35, and 36 should be attributed to MODIS. For bands 23, 24, and 25, however, the scan asymmetry of the MODIS observations is physical, the observed AIRS-MODIS differences are symmetric with scan angle, and these MODIS bands are expected to have good calibration accuracy as a function of scan angle. Therefore, regarding

the source of the AIRS-MODIS differences observed as a function of scan angle for these shorter wavelength bands, these analyses are not conclusive and further investigation is required.

[24] Figure 10 displays the AIRS-MODIS differences as a function of solar zenith angle. (Note that the difference at 90° solar zenith angle is subtracted from the plotted values). Larger solar zenith angles are local nighttime and smaller angles are local daytime. Noting that solar zenith angles of ~60 to ~120° correspond to data collected near or over the colder polar regions, and considering the previously described scene temperature dependence of the observed differences, accounts for the behavior seen in Figure 10.

[25] The high accuracy of the comparisons presented here is made possible by the high spectral resolution of AIRS and careful filtering of spatially nonuniform scenes. With only small corrections to account for spectral gaps within the AIRS spectra, the AIRS spectra can simply be convolved with the broadband SRFs to create the comparisons. With the forthcoming generation of high-spectral resolution infrared observations from geostationary platforms, promise exists for making analogous comparisons with polar orbiting sensors to characterize the intersensor biases for the entire infrared global observing system. Currently, intercomparisons of the operational geostationary and polar orbiting broadband sensors are made routinely [Gunshor *et al.*, 2004]. The intercomparison of sensors on different platforms naturally requires a more selective geocolocation process than what is required for the comparison of sensors on the same platform. In addition, while the SRFs for many of the broadband operational sensors are similar, they are not the same, and the comparison technique must rely on the incorporation of computed radiances for each sensor. This limits the comparisons to clear sky scenes and more importantly introduces various absolute uncertainties (which are difficult to estimate) and decreases the absolute accuracy of the comparisons. AIRS observations are now being incorporated into the intercalibration project [Gunshor *et al.*, 2003]. As mentioned previously, the largest source of absolute uncertainty for the AIRS-MODIS differences presented here are due to spectral gaps in the AIRS spectra; this should be considered when selecting the spectral coverage and resolution of future sensors if accurate intersensor comparisons is a desired application.

5. Summary

[26] A detailed comparison of EOS Aqua AIRS and MODIS infrared radiances for spatially uniform scenes collected on 6 September 2002 and 18 February 2004 has been presented. An approach to account for spectral gaps in the AIRS spectra when convolving with the MODIS SRFs has been introduced. Estimates of the absolute uncertainty of the comparisons are 0.1 K or less for the majority of the MODIS bands. Mean differences between AIRS and MODIS are ~1 K or less for all bands and many bands show agreement of 0.1 K or better. At the same time, only band 22 (3.9 μm) shows good absolute agreement and no significant dependence on scene temperature, scan angle, or solar zenith angle. Differences for MODIS bands 27, 28, 34, 35, and 36 display clear and significant dependencies on

scene temperature. While not conclusive regarding the physical source of these differences, introduction of MODIS SRF spectral shifts for these bands greatly improves the agreement with AIRS. Small differences as a function of scan angle are also clearly defined; for the longwave CO₂ bands these differences are attributed to MODIS, while further investigation is required to determine the source(s) of error for bands 23, 24, and 25. Results for the 2 days are very similar, with changes in mean differences of 0.1 K or less for most bands.

[27] Continuation of this study will include AIRS-MODIS comparisons performed for 1 or more selected days per season per year, which will allow the biases to be tracked over the entire Aqua mission. We plan to incorporate longwave observations by Clouds and the Earth's Radiant Energy System (CERES) on Aqua into these comparisons. Following the launch of the National Polar Orbiting Environmental Satellite System (NPOESS) Preparatory Project platform, similar radiance comparisons between the high-spectral resolution Cross track Infrared Sounder (CrIS) and the high-spatial resolution Visible Infrared Imaging Radiometer Suite (VIIRS) will also be performed. Finally, comparisons performed using future observations from a high-spectral resolution infrared sensor in geostationary orbit are expected to lead to an improved understanding of intersensor biases for the entire infrared observing system.

[28] **Acknowledgments.** This research has been supported by the EOS Science Project Office under NASA contracts NAS5-31375 and NNG04GG31G and by the Integrated Program Office under contract 50-SPNA-1-00039. The authors would like to extend our thanks to Liam Gumley, Mat Gunshor, Paul van Delst, Allen Huang, George Aumann, and Paul Menzel for discussions regarding various aspects of this work.

References

- Aumann, H. H., et al. (2003), AIRS/AMSU/HSB on the Aqua Mission: Design, science objectives, data products, and processing systems, *IEEE Trans. Geosci. Remote Sens.*, *41*, 253–264.
- Barnes, W. L., T. S. Pagano, and V. V. Salomonson (1998), Prelaunch characteristics of the Moderate resolution Imaging Spectroradiometer (MODIS) on EOS-AM1, *IEEE Trans. Geosci. Remote Sens.*, *36*, 1088–1100.
- Goldberg, M., T. King, W. Wolf, C. Barnet, H. Gu, and L. Zhou (2004), Using MODIS with AIRS to develop an operational cloud-cleared radiance product, paper presented at Fourth International Asia-Pacific Environmental Remote Sensing Symposium, Remote Sensing of the Atmosphere, Ocean, Environment, and Space, Int. Soc. for Opt. Eng., Honolulu, Hawaii, 8–11 Nov.
- Goody, R., and R. Haskins (1998), Calibration of radiances from space, *J. Clim.*, *11*, 754–758.
- Gunshor, M. M., D. Tobin, T. J. Schmit, and W. P. Menzel (2003), First satellite intercalibration comparing high spectral resolution AIRS with operational geostationary imagers, paper presented at 12th Conference on Satellite Meteorology and Oceanography, Am. Meteorol. Soc., Long Beach, Calif., 9–13 Feb.
- Gunshor, M. M., T. J. Schmit, and W. P. Menzel (2004), Intercalibration of the infrared window and water vapor channels on Operational Geostationary Environmental Satellites using a single polar orbiting satellite, *J. Atmos. Oceanic Technol.*, *21*, 61–68.
- Huang, H.-L., and W. L. Smith (2004), Apperception of clouds in AIRS data, paper presented at Workshop on Assimilation of High Spectral Resolution Sounders in NWP, Eur. Cent. for Med.-Range Weather Forecasts, Reading, U. K., 28 June to 1 July.
- Larar, A., W. L. Smith, H. E. Revercomb, J. Taylor, D. K. Zhou, R. O. Knuteson, and S. Mango (2005), Analysis of infrared spectral radiance observed during EAQUATE and other recent NAST field campaigns, paper presented at Topical Meeting, Hyperspectral Imaging and Sounding of the Environment, Opt. Soc. of Am., Alexandria, Va., 31 Jan. to 3 Feb.

- Li, J., W. P. Menzel, F. Sun, T. J. Schmit, and J. Gurka (2004a), AIRS sub-pixel cloud characterization using MODIS cloud products, *J. Appl. Meteorol.*, *43*, 1083–1094.
- Li, J., W. P. Menzel, W. Zhang, F. Sun, T. J. Schmit, J. J. Gurka, and E. Weisz (2004b), Synergistic use of MODIS and AIRS in a variational retrieval of cloud parameters, *J. Appl. Meteorol.*, *43*, 1619–1634.
- Li, J., H.-L. Huang, C.-Y. Liu, P. Yang, T. J. Schmit, H. Wei, E. Weisz, and W. P. Menzel (2005a), Retrieval of cloud microphysical properties from MODIS and AIRS, *J. Appl. Meteorol.*, *44*, 1526–1543.
- Li, J., C.-Y. Liu, H.-L. Huang, T. J. Schmit, X. Wu, W. P. Menzel, and J. J. Gurka (2005b), Optimal cloud-clearing for AIRS radiances using MODIS, *IEEE Trans. Geosci. Remote Sens.*, *43*(6), 1266–1278.
- McClatchey, R. A., R. W. Fenn, J. E. A. Selby, F. E. Voltz, and J. S. Garing (1972), Optical properties of the atmosphere, *Environ. Res. Pap. AFCRL-72-0497*, Air Force Cambridge Res. Lab., Bedford, Mass.
- Moeller, C. C., H. E. Revercomb, S. A. Ackerman, W. P. Menzel, and R. O. Knuteson (2003a), Evaluation of MODIS thermal IR band L1B radiances during SAFARI 2000, *J. Geophys. Res.*, *108*(D13), 8494, doi:10.1029/2002JD002323.
- Moeller, C. C., R. O. Knuteson, D. C. Tobin, H. E. Revercomb, and W. P. Menzel (2003b), Assessment of Aqua MODIS and AIRS TIR band L1B radiances using ER-2 based observations during TX-2002, Earth Observing Systems VII, 3–6 August 2003, *Proc. SPIE Int. Soc. Opt. Eng.*, *5151*, 355–366.
- Pagano, T. S., H. H. Aumann, and L. L. Strow (2000), Pre-launch performance characteristics of the Atmospheric Infrared Sounder (AIRS), *Proc. SPIE Int. Soc. Opt. Eng.*, *4169*, 268–278.
- Pagano, T. S., H. H. Aumann, D. E. Hagan, and K. Overoye (2003), Pre-launch and in-flight radiometric calibration of the Atmospheric Infrared Sounder (AIRS), *IEEE Trans. Geosci. Remote Sens.*, *41*, 265–273.
- Parkinson, C. L. (2003), Aqua: An Earth-observing satellite mission to examine water and other climate variables, *IEEE Trans. Geosci. Remote Sens.*, *41*, 173–183.
- Revercomb, H. E., et al. (2003), Atmospheric Infrared Sounder (AIRS) validation with the S-HIS (Scanning High-resolution Interferometer Sounder), ORS/FTS Topical Meeting, Opt. Soc. of Am., Quebec City, Que., Canada, 3–6 Feb.
- Smith, W. L., D. K. Zhou, H. L. Huang, J. Li, X. Liu, and A. M. Larar (2004), Extraction of profile information from cloud contaminated radiances, paper presented at ECMWF Workshop on Assimilation of High Spectral Resolution Sounders in NWP, Eur. Cent. for Med.-Range Weather Forecasts, Reading, U. K., 28 June to 1 July.
- Strow, L. L., S. E. Hannon, S. De Souza-Machado, H. E. Motteler, and D. C. Tobin (2003a), An overview of the AIRS radiative transfer model, *IEEE Trans. Geosci. Remote Sens.*, *41*, 303–313.
- Strow, L. L., S. E. Hannon, M. Weiler, K. Overoye, S. L. Gaiser, and H. H. Aumann (2003b), Prelaunch spectral calibration of the Atmospheric Infrared Sounder (AIRS), *IEEE Trans. Geosci. Remote Sens.*, *41*, 274–286.
- Tobin, D. C., H. E. Revercomb, S. A. Ackerman, P. Antonelli, M. M. Gunshor, R. O. Knuteson, and C. C. Moeller (2003), Characterization of Atmospheric Infrared Sounder (AIRS) Earth scene radiances, paper presented at ORS/FTS Topical Meeting, Opt. Soc. of Am., Quebec City, Que., Canada, 3–6 Feb.
- Tobin, D. C., et al. (2006), Radiometric and spectral validation of Atmospheric Infrared Sounder observations with the aircraft-based Scanning High-Resolution Interferometer Sounder, *J. Geophys. Res.*, *111*, D09S02, doi:10.1029/2005JD006094.
- Wan, Z., Y. Zhang, Q. Zhang, and Z.-L. Li (2004), Quality assessment and validation of the MODIS global land surface temperature, *Int. J. Remote Sens.*, *25*, 261–274.
- Weinreb, M. P., M. Jamison, N. Fulton, Y. Chen, J. X. Johnson, J. Bremer, C. Smith, and J. Baucom (1997), Operational calibration of Geostationary Operational Environmental Satellite-8 and -9 imagers and sounders, *Appl. Opt.*, *36*, 6895–6904.
- Xiong, X., K. Chiang, B. Guenther, and W. L. Barnes (2002), MODIS thermal emissive bands calibration algorithm and on-orbit performance, *Proc. SPIE*, *4891*, 255–263.
- Xiong, X., K. Chiang, J. Esposito, B. Guenther, and W. L. Barnes (2003), MODIS on-orbit calibration and characterization, *Metrologia*, *40*, 89–92.

C. C. Moeller, H. E. Revercomb, and D. C. Tobin, Cooperative Institute for Meteorological Satellite Studies, Space Science and Engineering Center, University of Wisconsin, Madison, WI 53706, USA. (dave.tobin@ssec.wisc.edu)

T. S. Pagano, NASA Jet Propulsion Laboratory, Pasadena, CA 91109, USA.